



Available online at www.sciencedirect.com

ScienceDirect

Advances in Space Research 65 (2020) 95-106

ADVANCES IN SPACE RESEARCH (a COSPAR publication)

www.elsevier.com/locate/asr

Characteristics of equatorial nighttime spread F – An analysis on season-longitude, solar activity and triggering causes

Ephrem Beshir ^{a,1}, Melessew Nigussie ^b, Mark B. Moldwin ^c

^a Space Science and Application Research Development Department, Entoto Observatory and Research Center (EORC), Ethiopian Space Science and Technology Institute (ESSTI), Addis Ababa, Ethiopia

^b Washera Geospace and Radar Science Laboratory, Physics Department, Bahir Dar University, Bahir Dar, Ethiopia ^c Climate and Space Sciences and Engineering, University of Michigan, USA

Received 14 May 2019; received in revised form 9 September 2019; accepted 11 September 2019 Available online 25 September 2019

Abstract

To understand global variability and triggering mechanisms of ionospheric nighttime equatorial spread F (ESF), we analyzed measurements from satellite and a ground-based GPS station for the years between 2010 and 2017. In this study we present seasonal-longitudinal as well as monthly variability of ESF occurrence for solar minimum and yearly variations of ESF occurrence for solar maximum and minimum periods. One of the long standing open questions in the study of ESF is what exactly initiates the Rayleigh-Taylor (RT) plasma instability growth. This question is the focus of the present work. Zonal background eastward electric field and E × B upward plasma drift speed patterns are found to be critically important in understanding plasma irregularity formation. In addition to particular patterns observed on these parameters, the background plasma density in the local evening hours just before the onset of ESF occurrence is very important. Stronger plasma densities just before the onset of irregularities resulted in stronger plasma irregularities, while relatively less dense plasma just before the onset of irregularities resulted in relatively lower plasma irregularities. Seasonal variations in ESF activity between March and September equinox seasons with comparable plasma densities can be defined in terms of the rate of change of solar flux F10.7 (dF10.7/day) index. Strongest ESF occurrence and strongest dF10.7/day are measured in the same month out of all other months in 2016 and 2017. Longitudinal variations of ESF activity in our measurements are related to longitudinal variations of plasma densities. We also found that ESF occurrence is better correlated with rate of change of F10.7 index for months in equinox seasons than for months in solstice seasons for the years between 2013 and 2016.

Keywords: ESF; Zonal eastward electric field; E × B; IEF_y; ROTI; RODI; F10.7

1. Introduction

The equatorial F region of the Earth's ionosphere is known for its peculiar characteristics immediately after sunset. Dense plasma moves to high altitude because of $E \times B$ upward plasma drift resulting in plasma density instability. Density perturbations at F_2 bottom side causes

movement of low density plasma into dense plasma resulting in irregular plasma density in the F-region of the ionosphere. Equatorial spread F (ESF) corresponds to electron density irregularities observed in the nighttime ionosphere of the equatorial region. It has been an active research topic in space science studies due to its impact on radio communications since its first discovery by Booker and Wells (1938). Although ESF has been extensively studied, the exact triggering causes of its formation and its variability are not known very well.

Department of Physics, University of Samara, Samara, Ethiopia.

E-mail addresses: biboephy@gmail.com (E. Beshir), mmoldwin@umich.edu (M.B. Moldwin)

ESF formation and its variability is known to depend on a number of parameters that makes it a complex problem. One of the main causes for the formation of nighttime ionospheric plasma irregularity is the prereversal enhancement (PRE) electric field. PRE is an enhancement in the eastward electric field in the E-region of the ionosphere that is caused by a high conductivity gradient across the day night terminator during the post-sunset hours (Farley et al., 1986). This enhancement occurs just before the reversal of eastward electric field during day time to westward during nighttime around 20:00 LT (Tsunoda, 1980). Since the eastward electric field reaches maximum around this hour, upward E × B plasma drift speed becomes maximum causing stronger plasma in F₂ region to reach to higher altitudes resulting in denser plasma at the top of less dense plasma, which is favorable for generation of plasma bubbles and finally formation of ESF. Fast instability growth as a result of an enhancement in PRE electric field is confirmed by many studies (Woodman and La Hoz, 1976; McClure et al., 1977; Tsunoda, 1980). Using incoherent scatter radar, Basu et al. (1996) and Huang (2018) concluded that post-sunset upward plasma drift of 20 m/s is a threshold value for the occurrence of ESF. But according to Huang (2018), this drift value varies depending on season and solar flux level. Although upward plasma drift is very important for the occurrence of ESF, factors like gravity waves, F2 bottom side perturbations and neutral winds are known to affect ESF occurrence. For instance Röttger (1973), Kelley et al. (1981) and Tsunoda et al. (1981) confirmed that gravity waves play an important role in plasma irregularity generation and in its day to day variability. Mendillo et al. (1992), Maruyama and Matuura (1984) and Seba et al. (2018) showed that transequatorial wind suppresses the formation of ESF. In addition to this transequatorial wind, vertical winds are also associated with ESF occurrence. According to Sekar and Raghavarao (1987) and Raghavarao et al. (1992), a vertical wind can result in polarized vertical electric field thereby directly affecting the plasma instability growth rate. Also during geomagnetic storms, prompt penetrating electric fields (PPEFs) are found to significantly affect the low-latitude and equatorial electric fields thereby affecting ESF formation (Schunk and Sojka, 1996; Abdu, 1997). Seba and Nigussie (2016) reported that a storm time PPEF can either trigger or inhibit occurrence of ESF depending on its direction. The onset and growth of plasma instability is widely known to be governed by the Rayleigh-Taylor (RT) plasma instability mechanism. Whose growth rate is given by Sekar and Raghavarao (1987)

$$\gamma = 1/L\{[g/v_{in}] + [E_x/B] + [W_x(v_{in}/\Omega_i)] - W_z\}$$

$$1/L = (1/Ni)(dNi/dz)$$
(1)

where L is the scale height of the plasma density in the bottom side F region, Ni is the electron/ion density, g is Earth's gravity, ν is ion-neutral collision frequency, $E \times B$ is the zonal electric field, B is geomagnetic field, Ω_i

is the ion gyro frequency and W_x and W_z are the zonal and vertical winds respectively. Since the ratio v_{in}/Ω_i is small (1/200) at 260 km and decreases exponentially with height, the zonal wind contribution is not significant (Chiu and Straus, 1979). The vertical component is found to be very important in occurrence of ESF. Raghavarao et al. (1992) showed that 20 m/s upward (downward) vertical wind at F-region altitudes can accelerate the generation of ESF significantly faster than the ESF generation when there is gravity (g) alone. Any source that strengthens zonal eastward electric field E_x can initiate the irregularity growth rate resulting in ESF formation. Although much work has been done about the nature and formation of ESF, the exact cause that initiates the plasma instability growth rate is the least known aspect in the study of ESF (Abdu et al., 2009).

ESF is known to show seasonal, longitudinal and solar cycle variability. The seasonal dependence and longitudinal variability is well documented (Burke et al., 2004a,b; Stolle et al., 2006; Su et al., 2006; Gentile et al., 2006). Also according to Burke et al. (2004b), the strongest and weakest equatorial plasma bubbles (EPB) are observed in the Atlantic-African longitude and Indian-Pacific sectors, respectively. Longitudinal variability is documented by many studies, but the mechanism for the longitudinal variability of ESF occurrence is unclear (Saito and Maruyama, 2007), while a solar cycle dependence of ESF occurrence is found (Abdu et al., 1985; Huang et al., 1987; Rao et al., 1997).

This work aims at studying one of the long standing questions, - what causes the RT plasma instability growth that results in ESF formation during different seasons.

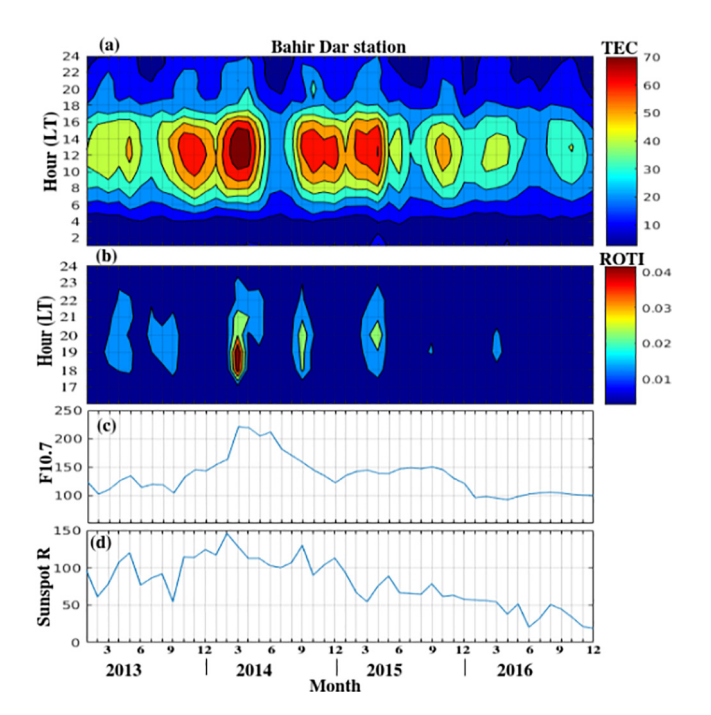


Fig. 1. TEC, ROTI, F10.7 and sunspot number R for the years between 2013 and 2016.

Global and seasonal variations and solar radiation flux dependence of nighttime equatorial plasma irregularities are also presented. Swarm and Communication/Navigation Outage Forecasting System (C/NOFS) satellite and ground-based GPS data from a dip geomagnetic equatorial station are utilized.

2. Data analysis

Ground-based GPS data from a geomagnetic dip equatorial station (Bahir Dar station (Bdmt), geomagnetic latitude 2.8, geomagnetic longitude 109.2, GMT + 3) and satellite data from C/NOFS, Swarm and high-resolution OMNI solar wind data are used in our study. Rate of

TEC (ROT) index measures small scale variations in TEC in units of TECU/min (1 TECU = 10^{16} electrons/ m^2). Bahir Dar ground-GPS station collects TEC data every 30 s. Therefore Δt_G in ROT calculations in our case is 30 s. Rate of vTEC index (ROTI) measures the standard deviation of ROT and is given by Eq. (3). In our ROTI calculations, the standard deviations of ROT are sampled in 5 min intervals since the 5 min interval is better for high time resolutions as recommended by Pi et al. (1997).

$$ROT = \left(\frac{vTEC}{\Delta t_G}\right)_{\Delta t_G = 30sec} \tag{2}$$

$$ROTI = \sqrt{\langle ROT^2 \rangle + \langle ROT \rangle^2}$$
 (3)

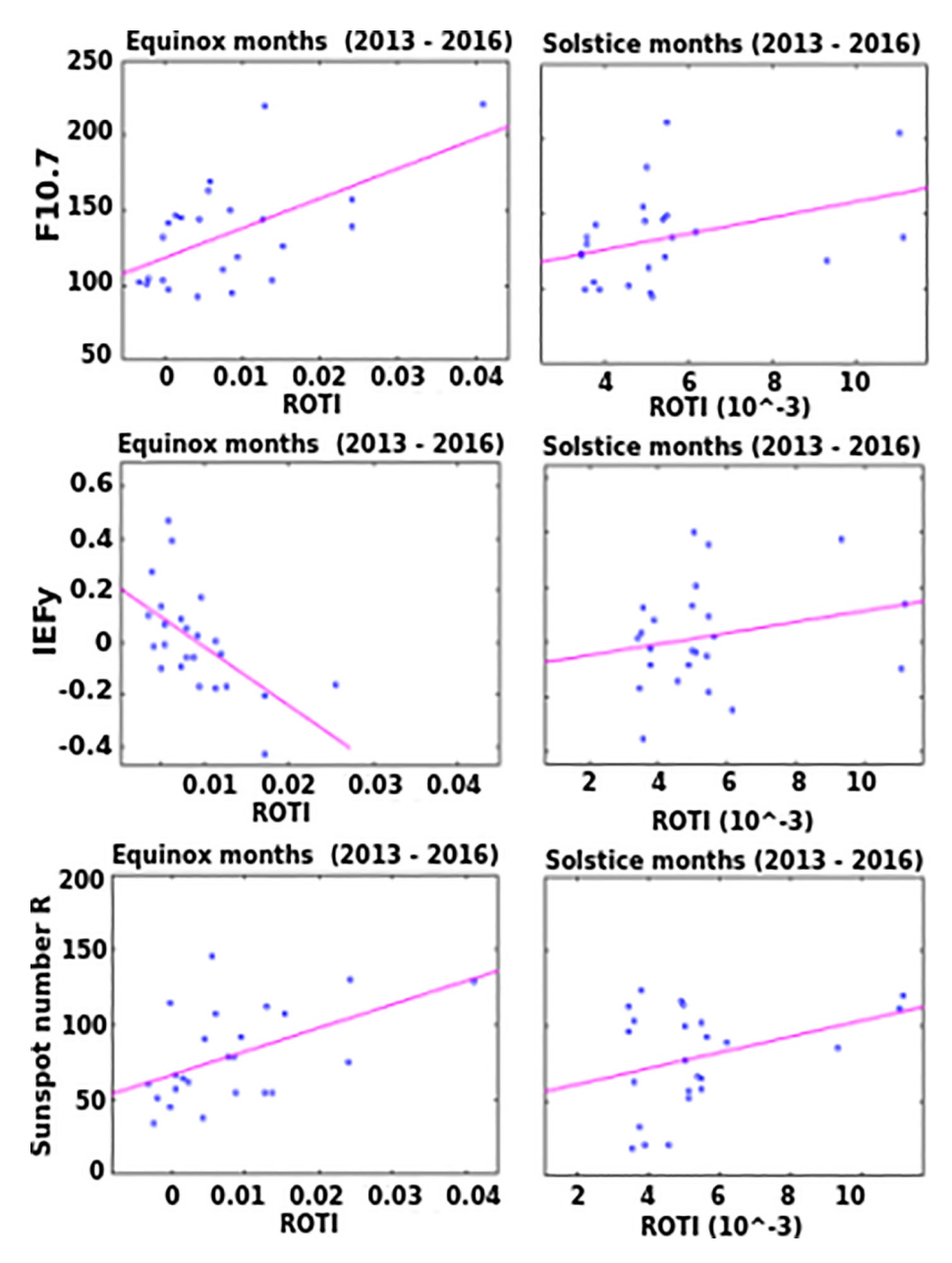


Fig. 2. Correlation of F10.7, IEFy and sunspot number R with ROTI in equinox and solstice seasons for the years between 2013 and 2016.

$$ROD = \left(\frac{\Delta Ni}{\Delta t_{SW}}\right)_{\Delta t_{SW} = 0.5 sec} \tag{4} \label{eq:ROD}$$

$$RODI = \sqrt{\langle ROD^2 \rangle + \langle ROD \rangle^2}$$
 (5)

where vTEC is vertical total electron content of the ionosphere and Ni is the density of the ionospheric plasma per unit cm³ as measured by the three Swarm satellites. Similarly rate of density (ROD) measures variations of electron density over the small scale. Since the time between every successive measurements in Swarm is half a second, Δt_{SW} in ROD (see Eq. (4)) calculations is half a second. The rate of density index (RODI), measures the standard deviation of ROD, which indicates the occurrence of ESF. It is calculated by using Eq. (5). In our RODI calculations, the standard deviations of ROD are sampled every 5 s interval. In Swarm satellite data measurements in Section 3.1, the longitudes are averaged for every 15 degrees and the latitudes are averaged for every three degrees (75 to 100 data points averaged). East-west interplanetary electric field (IEFy), sunspot number R and F10.7 index data are obtained from OMNI data center. E × B plasma drift speed, zonal electric field and plasma density data (for discussions in Section 3.2) are obtained from C/NOFS data center. IEF_v is mathematically expressed as $IEF_y = -V_{SW} \times B_Z$, where V_{SW} is the solar wind speed and Bz is the interplanetary magnetic field (IMF) z-component.

3. Results and discussion

3.1. ESF characteristics

Fig. 1 depicts yearly variation of vertical total electron content (vTEC) and nighttime spread F occurrence using the ground-based GPS station at the dip geomagnetic equatorial station in association with solar radiation flux level and sunspot number R for the years between 2013 and 2016. It shows monthly variations of vTEC, ROTI, F10.7 and sunspot number R at different hours. The vTEC

at this dip magnetic equatorial station is strongest during noon hours for all these years (see Fig. 1(a)).

The ROTI, which is an indicator of the occurrence of the nighttime ESF, is found to be strongest during the post-sunset hours between 18 and 20 local times (LT) (see Fig. 1(b)). The F10.7 solar flux index and sunspot R show that solar activity is maximum in the year 2014 and decays as the cycle proceeds to the next solar minimum period (see Fig. 1(c) and (d)). Correlation plots in Fig. 2 are monthly averaged data for equinox and solstice seasons for four years between 2013 and 2016. Equinox seasons in each year include six months (February, March, April, August, September and October) while solstice seasons include (May, Jun, July, November, December and January). Rate of change of F10.7 index (dF10.7/day) is daily variation of solar flux index calculated by subtracting suc-

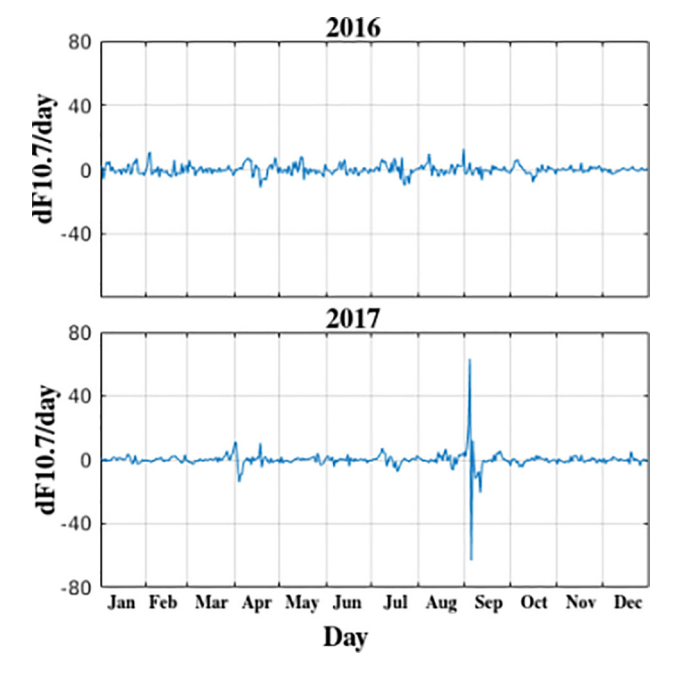


Fig. 4. Daily variations of F10.7 (dF10.7/day) in 2016 and 2017.

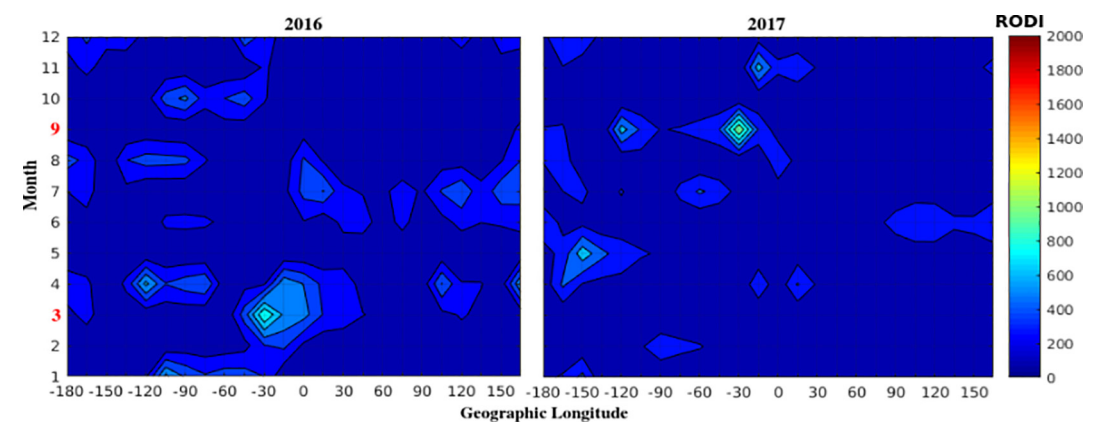


Fig. 3. Monthly variation of ESF as indicated by RODI for different longitude sectors from Swarm satellite measurements.

cessive daily means of F10.7 values. The correlation among vTEC, ROTI, F10.7, IEF_y (interplanetary electric field) and sunspot R can be seen on Fig. 2. ROTI better correlates with IEF_y, F10.7 and sunspot number R with correlation coefficients of -0.59, 0.58 and 0.51, respectively

for months during equinox season than for months in solstice seasons. More results and discussions on this are presented in Section 3.2.

Longitudinal-monthly variations for these two years at solar minimum shown in Fig. 3 indicates that relatively

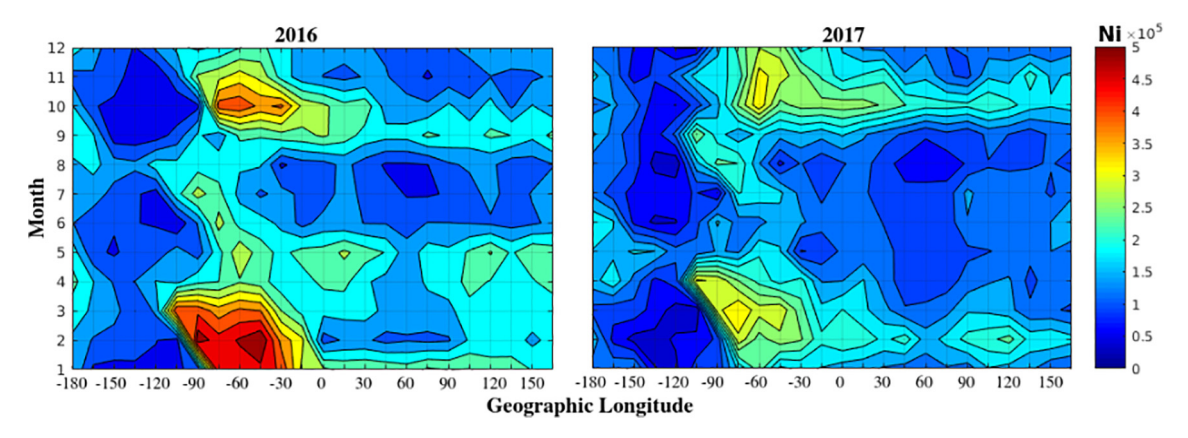


Fig. 5. Monthly plasma density (Ni) for the years 2016 and 2017 from Swarm satellite measurements.

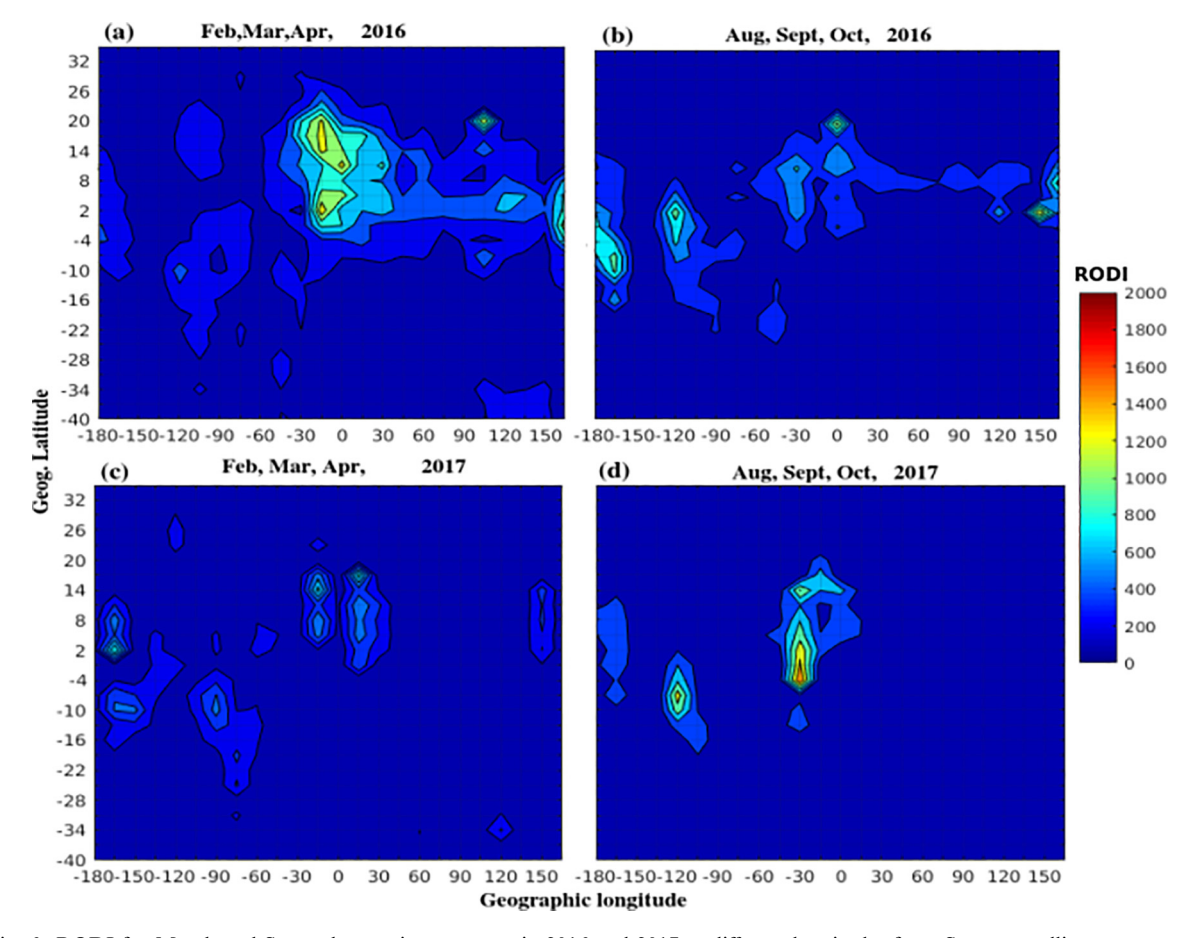


Fig. 6. RODI for March and September equinox seasons in 2016 and 2017 at different longitudes from Swarm satellite measurements.

strongest ESF activity is measured in September 2017 in the Atlantic sector (≈0 to −45 degree longitude) than in other months and longitudinal sectors in 2016 and 2017. Similarly the strongest dF10.7/day is measured in September 2017 (see Fig. 4). That is the strongest ESF activity and the strongest dF10.7/day measured in the same month (September 2017). This indicates the importance of dF10.7/day in the variability of ESF. Many studies showed that ionospheric parameters like NmF2, foF2 and TEC linearly increase with F10.7 index up to some saturation level (Bhuyan et al., 1983; Lakshmi et al., 1988; Balan et al., 1994). Therefore change in F10.7 index which results in change in electron density of the ionosphere can be an important parameter in the study of ESF variability.

Monthly-longitudinal plasma density for the years 2016 and 2017 is shown in Fig. 5. It shows that the plasma density is stronger in the two equinox seasons in both 2016 and 2017 than other seasons in the American-African sector. Figs. 6 and 7 show seasonal-longitudinal variations of ESF occurrence for two years at solar minimum (2016 and 2017) as measured by the three Swarm satellites for the evening hours between 18 LT and 01

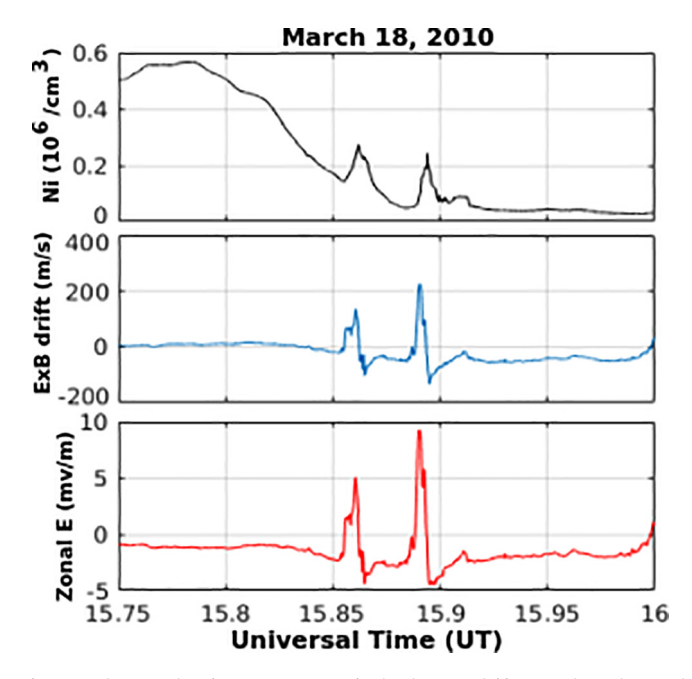


Fig. 8. Plasma density, $E \times B$ vertical plasma drift speed and zonal electric field on March 18, 2010 measured from C/NOFS satellite.

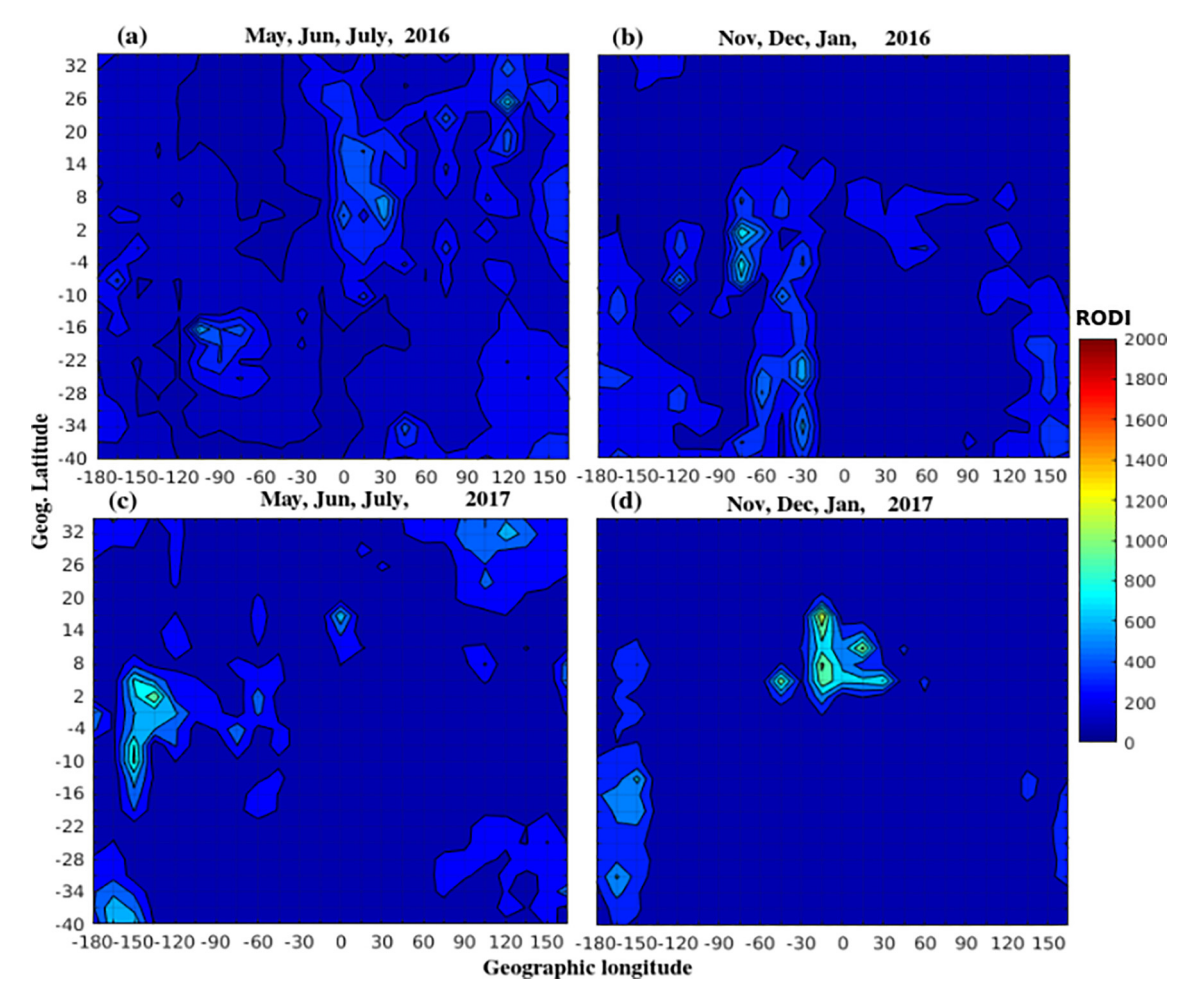


Fig. 7. RODI for June and December solstice seasons in 2016 and 2017 at different longitudes from Swarm satellite measurement.

LT. The comparison between March equinox seasons in 2016 and 2017 in Fig. 6(a & b) shows that RODI measurements in 2016 are greater than that of RODI measurements in 2017, especially in the Atlantic sector. Significant work

has been done to determine why ESF activity shows variations during the two equinox seasons (March and September). The March equinox season in 2016 showed strongest seasonal mean of plasma density over all longitudes equal

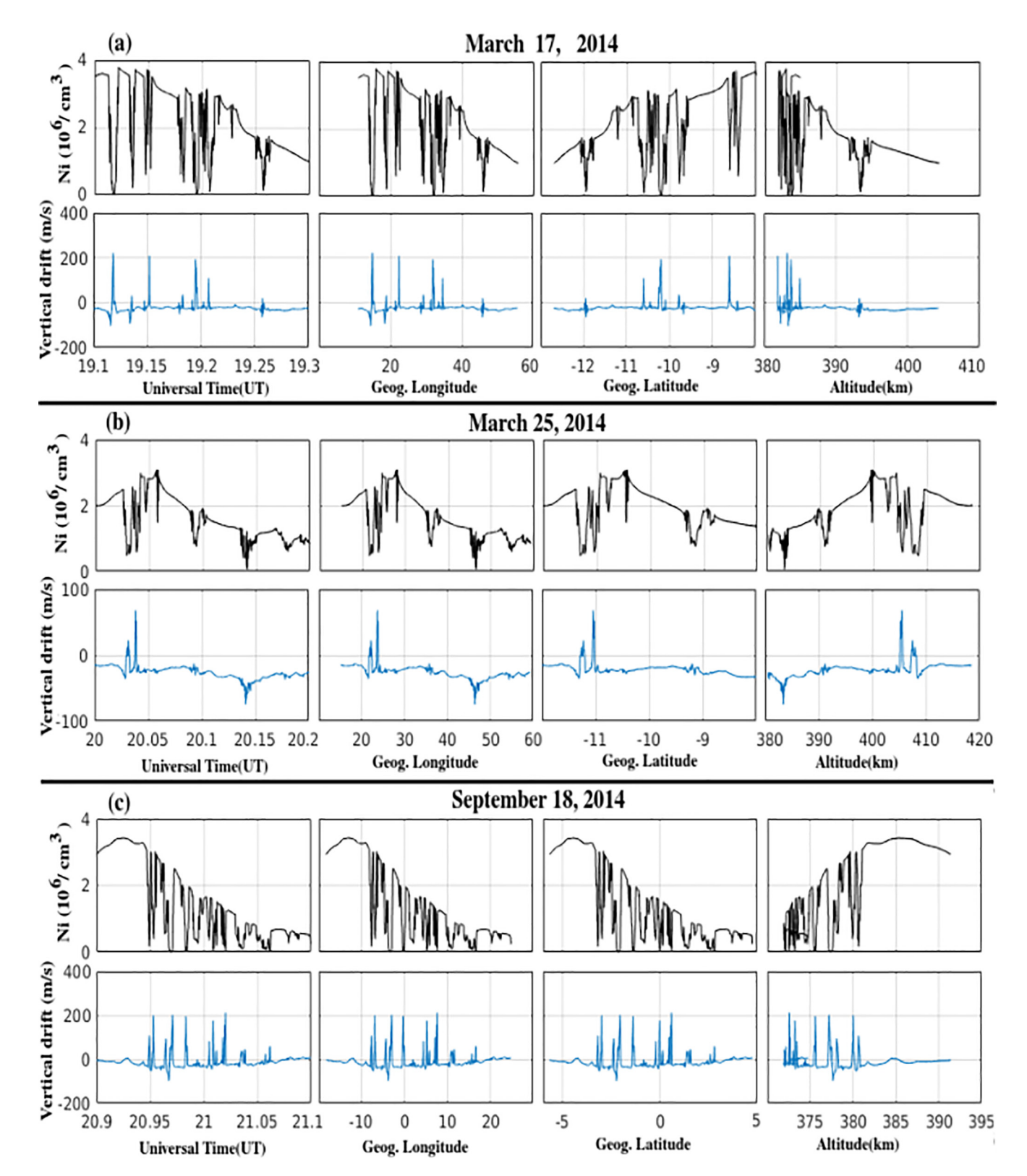


Fig. 9. Electron density and vertical plasma drift on March 17, 25 and September 18, 2014 measured from C/NOFS satellite as a function of longitude, latitude and altitude.

to 2.2×10^5 ions/cm³ and strongest seasonal mean of RODI over all longitudes equal to 219 (see Figs. 5 and 6) than the other seasons in both 2016 and 2017. In 2017, March and September equinox seasons show comparable seasonal mean plasma densities over all longitude sectors equal to 1.7×10^5 ions/cm³ and 1.5×10^5 ions/cm³ respectively. But the seasonal mean of dF10.7/day in March and September equinox seasons are 0.1 and 0.9 respectively (see Fig. 4). March and September equinox seasons in 2017 showed seasonal mean of RODI over all longitude sectors of 146 and 180 respectively. This greater seasonal mean of dF10.7/day in September 2017 may have resulted in greater ESF activity than March 2017. In solstice seasons in both 2016 and 2017 (see Figs. 4, 5 and 7), the ESF variability, plasma densities and F10.7 are not well correlated according to Swarm satellite measurements indicating that the variability and formation of ESF in solstice seasons are difficult for predictions. In discussions of Fig. 2 above, we also showed that ESF activity in equinox seasons is better correlated with solar activities than in solstice seasons from ground based GPS measurements. So solstice seasons are

not well correlated both in ground-based GPS and Swarm satellite-based measurements, while equinox seasons showed better correlations with solar activity both in ground- based GPS measurements and from Swarm satellite measurements.

Also the American-African longitudinal sector is found to display significantly larger Ni and RODI than the other longitudinal sectors in March equinox season in 2016. A similar result is obtained in Burke et al. (2004b). The existence of stronger ESF activity in African-Atlantic sector can be related to the existence of stronger plasma density in the American-African sector but the reason why the plasma density shows stronger magnitude in this region remains unclear.

3.2. ESF formation

The direct physical process that results in plasma density irregularities is one of the least known aspects in the study of ESF. C/NOFS satellite topside view of ionospheric density as a function of longitude, latitude and altitude and

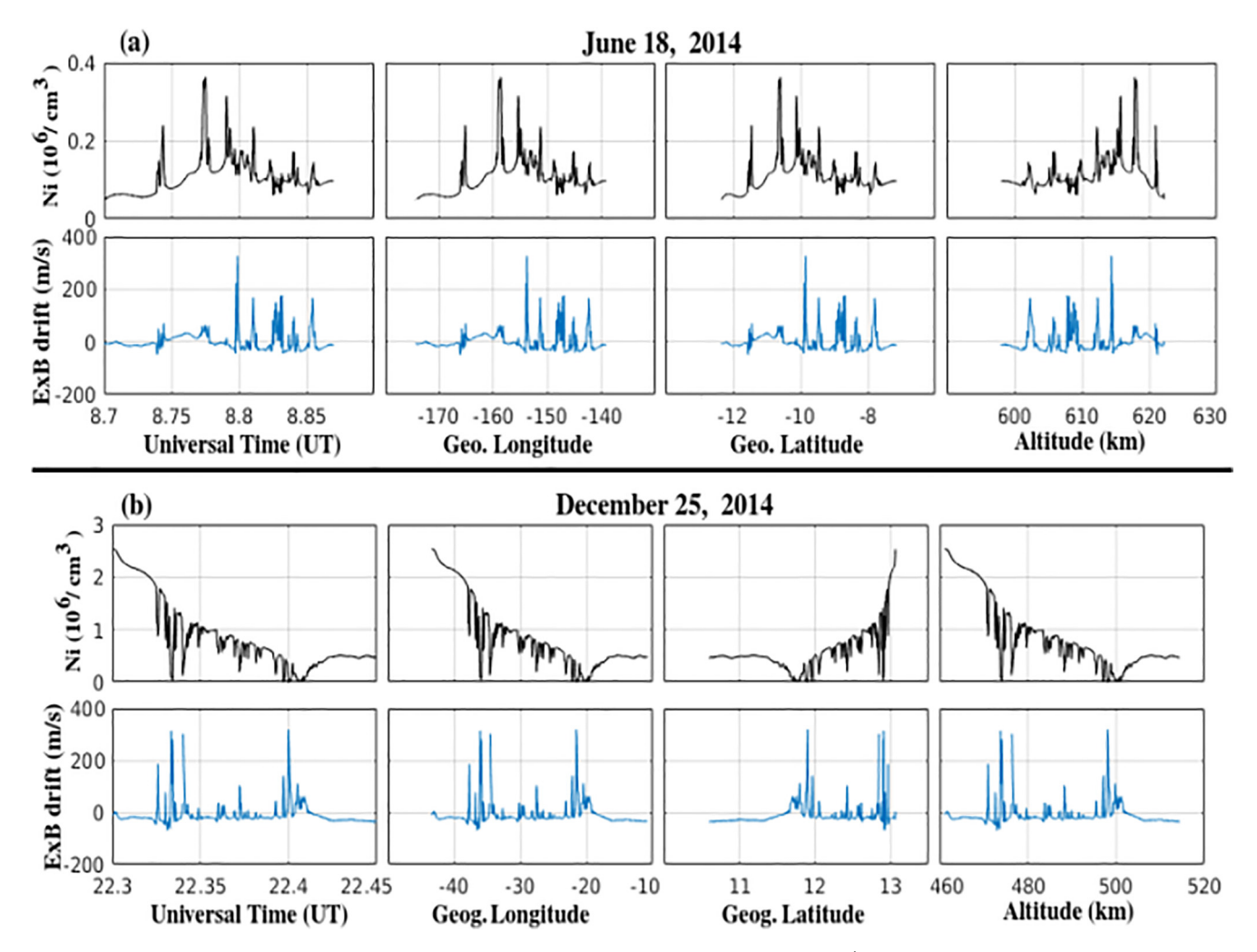


Fig. 10. Electron density and vertical plasma drift on June 18 and December 25, 2014 measured from C/NOFS satellite as a function of longitude, latitude and altitude.

vertical plasma drift speed as a function of longitude, latitude and altitude allows examination of conditions that may be related to the triggering of ESF formation.

Fig. 8 shows the relation between zonal electric field, upward plasma drifts and plasma density for the evening hours between 22.28 LT and 2.19 LT. It clearly indicates that short time fluctuations in zonal electric field and upward plasma drift speed (V_Z) are very well associated with plasma density fluctuations. Since zonal electric field is directly proportional to upward plasma drift, a change in the electric field can result in a change in plasma drift

speed. The black plots in Figs. 9 and 10 show plasma density (Ni) fluctuations that resulted due to polarization electric field within the plasma depletions (bubbles). The corresponding local times for March 17, March 25 and September 18 in Fig. 8 are between 19.8 LT to 23 LT, 21 LT to 0.15 LT and 19.68 LT to 22.76 LT respectively.

The plots also indicate that strong density fluctuations and upward plasma speed fluctuations occurred at the same time, longitude, latitude and altitude. This indicates that one of the potential causes of ESF occurrence during the nighttime is related to upward $E \times B$ plasma drift speed

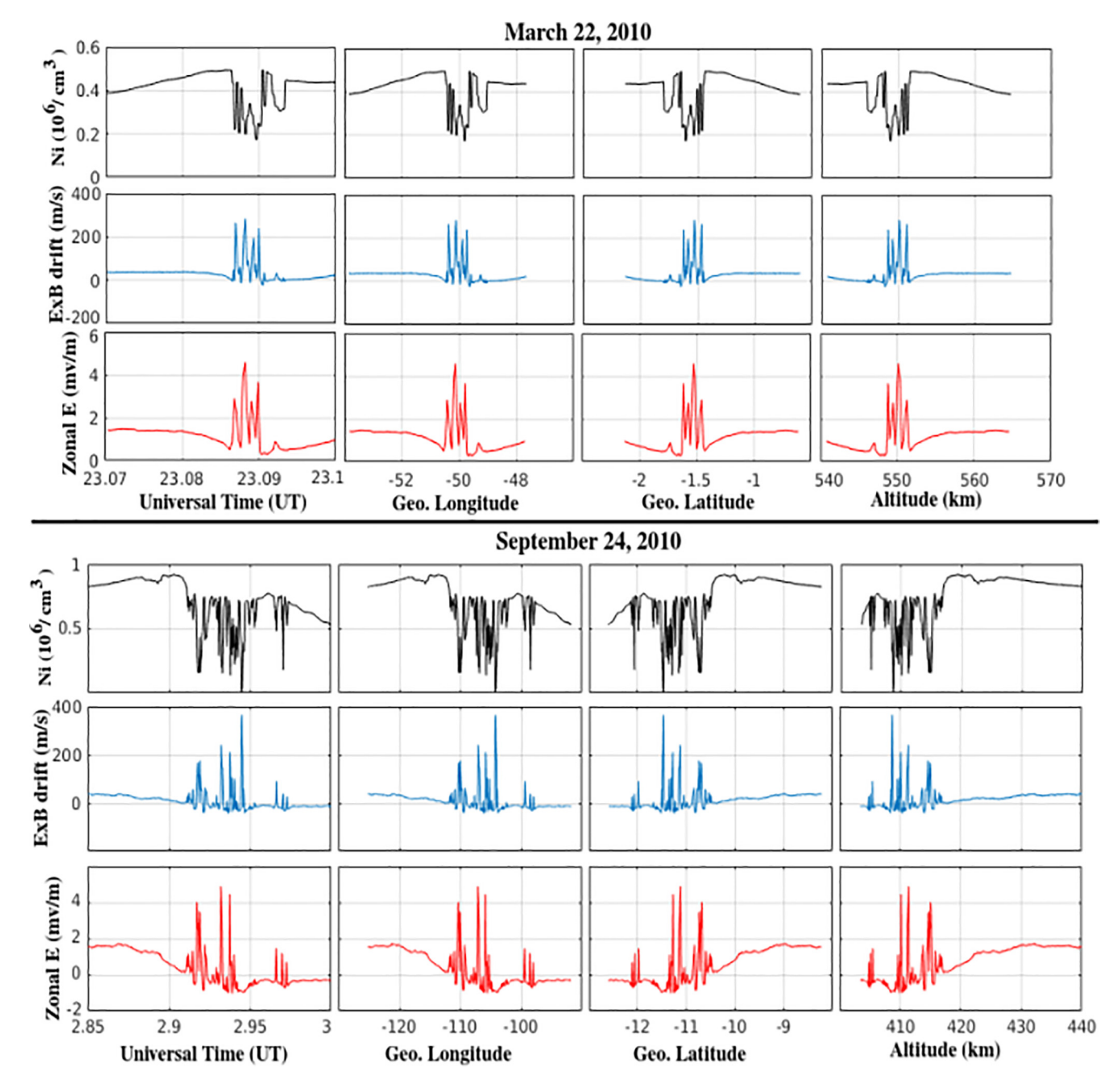


Fig. 11. Electron density, vertical plasma drift and zonal electric field on March 22 and September 24, 2010 measured from C/NOFS satellite as a function of longitude, latitude and altitude.

Table 1 Summary of $E \times B$ vertical plasma drift and ionospheric plasma density.

Days	$\Delta E \times B$ vertical drift (m/s)	Ni (initial) (10 ⁶ /cm ³)	$\Delta Ni (10^6/cm^3)$	Time (UT)	Time (LT)
March 21, 2010	214	0.69	-0.51	01:52:31-01:52:53	20:40:24-20:40:36
March 24, 2010	165	0.262	-0.092	04:13:08-04:13:20	20:03:02-20:03:16
March 26, 2010	298	0.62	-0.48	03:09:06-03:09:18	20:45:27-20:45:39
March 27, 2010	173	0.29	-0.07	01:47:29-01:47:37	20:36:22-20:36:30
March 28, 2010	328	0.24	-0.11	02:09:06-02:09:12	22:23:14-22:23:20
September 25, 2010	170	0.59	-0.24	01:43:26-01:43:38	22:24:14-22:24:26
September 26, 2010	256	0.67	-0.51	01:47:29-01:47:41	19:45:27-19:45:39
September 27, 2010	331	0.4	-0.3	02:14:09-02:14:17	23:13:08-23:13:20
September 28, 2010	85	0.2821	-0.1196	07:18:11-07:18:23	22:45:27-22:45:39
September 29, 2010	82	0.94	-0.8	04:07:05-04:07:13	19:49:30-19:49:38
March 13, 2014	210	2.6	-1.85	13:41:25-13:41:37	20:45:27-20:45:39
March 14, 2014	267	2.9	-2.89	13:41:25-13:41:37	20:45:27-20:45:39
March 15, 2014	352	2.54	-2.48	13:21:13-13:21:33	19:52:32-19:52:52
March 16, 2014	277	3.3	-3.29	13:07:05-13:07:25	20:53:32-20:53:52
March 17, 2014	331	2.8	-2.79	11:15:09-11:15:21	20:41:25-20:41:37
June 16, 2014	55	0.2	0.11	09:34:21-09:34:29	23:10:06-23:10:14
June 17, 2014	106	0.12	0.1	09:13:08-09:13:16	23:17:10-23:17:18
June 18, 2014	193	0.1	0.14	08:48:29-08:48:37	22:43:26-22:43:34
September 17, 2014	222	2.8	-2.7	11:58:35-11:58:43	20:43:26-20:43:34
September 18, 2014	432	2.6	-2.53	13:04:03-13:04:11	20:04:03-20:04:11
September 20, 2014	360	2.2	-2.1	10:39:23-10:39:31	20:18:11-20:18:19
September 21, 2014	460	1.44	-1.41	14:57:34-14:57:42	20:36:22-20:36:30
September 22, 2014	481	1.5	-1.45	20:46:28-20:46:34	20:07:05-20:07:11
December 19, 2014	484	0.63	-0.6	19:27:17-19:27:25	19:10:06-19:10:14
December 21, 2014	130	0.52	-0.42	18:24:15-18:24:23	20:23:14-20:23:22
December 22, 2014	81	0.56	-0.46	17:55:33-17:55:41	21:47:28-21:47:36
March 18, 2015	101	1.1	-1	15:52:48-15:52:56	20:20:24-20:20:32
March 20, 2015	116	1.4	-1.2	16:01:12-16:01:20	20:38:24-20:38:32
March 21, 2015	83	1	-0.8	15:17:24-15:17:32	20:26:24-20:26:24
September 18, 2015	70	1	-0.7	04:06:36-04:06:44	20:05:24-20:05:32
September 19, 2015	398	0.7	-0.7	04:34:12-04:34:24	20:39:36-20:39:48
September 20, 2015	369	1	-1	10:03:36-10:03:44	21:34:12-21:34:20
June 18, 2015	438	0.8	-0.8	03:22:48-03:22:54	20:30:00-20:30:06
June 20, 2015	328	1	-1	07:42:36-07:42:44	20:10:48-20:10:56
June 21, 2015	73	1.1	-0.7	08:22:48-08:22:60	20:46:12-20:46:24

fluctuations. A sudden sharp and strong increase in upward $E \times B$ plasma drift around F_2 bottom side can result in density perturbations that causes movement of less dense plasma into the denser plasma thereby forming plasma irregularities (see Figs. 9–11). March 17, 25 and September 18, 2014 plots (see Fig. 9) are night time measurements between 19.8 to 23.0, 21 to 0.15 and 19.68 to 22.76 local times respectively. June 18 and December 25, 2014 in Fig. 10 are also nighttime measurements between 21.07 to 0.04 and 19.4 to 21.73 local times respectively.

Fig. 11 indicates the relationship among plasma density, vertical $E \times B$ plasma drift and zonal eastward electric field. March 22 and September 24, 2010 are nighttime measurements between 19.48 to 19.92 and 18.5 to 20.89 local times respectively. The red plots are zonal east-west electric fields with positive being eastward and the negative being westward. As can be seen from Fig. 11, sharp sudden fluctuations in zonal electric fields, $E \times B$ plasma drift speeds and plasma density occurred at the same time, longitude, latitude and altitude. This indicates that a sudden sharp (in the range of ~20 s interval) fluctuation in vertical $E \times B$ plasma drift speed and/or zonal electric field are/is

one of the potential causes for the onset of the nighttime

Stronger background plasma density just before the onset of ESF and stronger ESF occurrences are observed during equinox seasons than solstice seasons (see Figs. 9–11). That is just before the onset of irregularities, the plasma density is higher in March and September months but the plasma density is lower just before the onset of ESF in June and December. The amount of initial plasma density just before the onset of plasma density perturbations is also very important in the formation of stronger plasma irregularities in our measurements. Table 1 summarizes the relations between E × B plasma drift speed fluctuations and plasma density perturbations in the local evening hours in different years as indicated. Strongest plasma density perturbations occurred in March and September months in 2014, which is solar maximum period. Furthermore, stronger background plasma densities resulted in stronger density perturbations in March and September 2014. It can be seen from Figs. 9-11 and Table 1 that stronger plasma densities result in stronger ESF.

4. Conclusions

The characteristics of ESF occurrence and potential triggering mechanisms are studied in this work using a ground-based GPS receiver at the dip magnetic equator and satellite measurements from the three Swarm and C/NOFS satellites. Based on our analysis the following main conclusions are drawn.

- The E × B upward plasma drift and/or zonal eastward electric field fluctuations result in ESF formation. That is the electric field and/or upward E × B plasma drift speed fluctuations initiated ESF formations.
- The ESF occurred in March and September equinox seasons are found to be much larger than that of ESF occurring in June and December solstice seasons. Stronger background plasma density just before the onset of ESF and stronger ESF occurrences are observed during equinox seasons than solstice seasons. That is just before the onset of irregularities, the plasma density is higher in March and September months but the plasma density is lower just before the onset of ESF in June and December. The amount of initial plasma density just before the onset of plasma density perturbations is also very important in the formation of stronger plasma irregularities in our measurements.
- The strongest ESF occurrence and strongest dF10.7/day are measured in the same month (September 2017) based on Swarm satellite measurements. Although plasma density is directly related to ESF, the strength of the magnitude of dF10.7/day is also very important in the variability of ESF activity. Similar plasma densities in March and September equinox seasons showed difference in ESF activity and this difference in ESF activity is related to the difference in the rate of change of F10.7 (dF10.7/day).
- The American-African longitudinal sector showed strongest plasma densities and ESF activities. Although longitudinal variations of ESF activity in our measurements are related to longitudinal variations in plasma densities, the cause for longitudinal variation in plasma densities remains unclear.
- The post-sunset equatorial spread F occurrences measured from ROTI are better correlated with IEF_y, solar flux F10.7 and sunspot number R for months in equinox seasons than for months in solstice seasons for years between 2013 and 2016. The coefficient of correlation between IEF_y, F10.7 and sunspot number R with ROTI are found to be -0.59, 0.58 and 0.51 for equinox seasons respectively. The correlations in solstice seasons are weak.

Acknowledgment

The authors are grateful for free UNAVCO ground GPS station, C/NOFS, Swarm and OMNI web satellite data cen-

ters. Mark B. Moldwin was partially supported by NSF AGS-1450512. Melessew Nigussie was supported by the University of Michigan African Presidential Scholar (UMAPS) program and Air Force Office of Scientific Research, Air Force Material Command USAF under Award No. FA9550-16-1-0070. Ephrem B. Seba is also thankful for Samara university of Ethiopia and Ethiopian Space Science and Technology Institute for their financial support. We are also thankful for the reviewers of this paper.

References

- Abdu, M., 1997. Major phenomena of the equatorial ionosphere-thermosphere system under disturbed conditions. J. Atmos. Sol. Terr. Phys. 59 (13), 1505–1519. https://doi.org/10.1016/S1364-6826(96) 00152-6.
- Abdu, M., Kherani, E.A., Batista, I., De Paula, E., Fritts, D., Sobral, J., et al., 2009. Gravity wave initiation of equatorial spread f/plasma bubble irregularities based on observational data from the spreadfex campaign. Ann. Geophys 27 (7), 2607–2622. https://doi.org/10.5194/angeo-27-2607-2009.
- Abdu, M., Sobral, J., Nelson, O., Batista, I., 1985. Solar cycle related range type spread-f occurrence characteristics over equatorial and low latitude stations in Brazil. J. Atmos. Terr. Phys. 47 (8–10), 901–905. https://doi.org/10.1016/0021-9169(85)90065-0.
- Balan, N., Bailey, G., Moffett, R., 1994. Modeling studies of ionospheric variations during an intense solar cycle. J. Geophys. Res. Space Phys. 99 (A9), 17467–17475. https://doi.org/10.1029/94JA01262.
- Basu, S., Kudeki, E., Basu, S., Valladares, C., Weber, E., Zengingonul, H., Bhattacharyya, S., Sheehan, R., Meriwether, J., Biondi, M., et al., 1996. Scintillations, plasma drifts, and neutral winds in the equatorial ionosphere after sunset. J. Geophys. Res. Space Phys. 101 (A12), 26795–26809. https://doi.org/10.1029/96JA00760.
- Bhuyan, P., Tyagi, T. R., Singh, L., Somayajulu, Y., 1983. Ionospheric electron content measurements at a northern low midlatitude station through half a solar cycle. http://nopr.niscair.res.in/handle/ 123456789/36746.
- Booker, H., Wells, H., 1938. Scattering of radio waves by the f-region of the ionosphere. Terr. Magn. Atmos. Electr. 43 (3), 249–256. https://doi.org/10.1029/TE043i003p00249.
- Burke, W., Gentile, L., Huang, C., Valladares, C., Su, S., 2004a. Longitudinal variability of equatorial plasma bubbles observed by dmsp and rocsat-1. J. Geophys. Res.: Space Phys. 109 (A12). https://doi.org/10.1029/2004JA010583.
- Burke, W., Huang, C., Gentile, L., Bauer, L., 2004b. Seasonal-longitudinal variability of equatorial plasma bubbles. Technical report, Air Force Research Lab Hanscom AFB MA Space Vehicles Directorate. https://apps.dtic.mil/dtic/tr/fulltext/u2/a434546.pdf.
- Chiu, Y., Straus, J., 1979. Rayleigh-taylor and wind-driven instabilities of the nighttime equatorial ionosphere. J. Geophys. Res. Space Phys. 84 (A7), 3283–3290. https://doi.org/10.1029/JA084iA07p03283.
- Farley, D., Bonelli, E., Fejer, B.G., Larsen, M., 1986. The prereversal enhancement of the zonal electric field in the equatorial ionosphere. J. Geophys. Res. Space Phys. 91 (A12), 13723–13728. https://doi.org/ 10.1029/JA091iA12p13723.
- Gentile, L., Burke, W., Rich, F., 2006. A climatology of equatorial plasma bubbles from dmsp 1989–2004. Radio Sci. 41 (5). https://doi.org/10.1029/2005RS003340.
- Huang, C.-S., 2018. Effects of the postsunset vertical plasma drift on the generation of equatorial spread f. Prog. Earth Planet. Sci. 5 (1), 3. https://doi.org/10.1186/s40645-017-0155-4.
- Huang, Y.-N., Cheng, K., Huang, W.-T., 1987. Seasonal and solar cycle variations of spread f at the equatorial anomaly crest zone. J. Geomagn. Geoelec. 39 (11), 639–657. https://doi.org/10.5636/ jgg.39.639.

- Kelley, M., Larsen, M., LaHoz, C., McClure, J., 1981. Gravity wave initiation of equatorial spread f: A case study. J. Geophys. Res. Space Phys. 86 (A11), 9087–9100. https://doi.org/10.1029/JA086iA11p09087.
- Lakshmi, D., Reddy, B., Dabas, R., 1988. On the possible use of recent euv data for ionospheric predictions. J. Atmos. Terr. Phys. 50 (3), 207–213. https://doi.org/10.1016/0021-9169(88)90069-4.
- Maruyama, T., Matuura, N., 1984. Longitudinal variability of annual changes in activity of equatorial spread f and plasma bubbles. J. Geophys. Res. Space Phys. 89 (A12), 10903–10912. https://doi.org/ 10.1029/JA089iA12p10903.
- McClure, J., Hanson, W., Hoffman, J., 1977. Plasma bubbles and irregularities in the equatorial ionosphere. J. Geophys. Res. 82 (19), 2650–2656. https://doi.org/10.1029/JA082i019p02650.
- Mendillo, M., Baumgardner, J., Pi, X., Sultan, P.J., Tsunoda, R., 1992. Onset conditions for equatorial spread f. J. Geophys. Res. Space Phys. 97 (A9), 13865–13876. https://doi.org/10.1029/92JA00647.
- Pi, X., Mannucci, A., Lindqwister, U., Ho, C., 1997. Monitoring of global ionospheric irregularities using the worldwide gps network. Geophys. Res. Lett. 24 (18), 2283–2286. https://doi.org/10.1029/ 97GL02273.
- Raghavarao, R., Sekar, R., Suhasini, R., 1992. Nonlinear numerical simulation of equatorial spread-feffects of winds and electric fields. Adv. Space Res. 12 (6), 227–230. https://doi.org/10.1016/0273-1177(92) 90061-2.
- Rao, P.R., Jayachandran, P., Ram, P.S., Rao, B.R., Prasad, D., Rose, K., 1997. Characteristics of vhf radiowave scintillations over a solar cycle (1983–1993) at a low-latitude station: Waltair (17.7 n, 83.3 e). Annales Geophysicae, vol. 15. Springer, pp. 729–733. https://doi.org/10.1007/s00585-997-0729-3.
- Röttger, J., 1973. Wave-like structures of large-scale equatorial spread-firregularities. J. Atmos. Terr. Phys. 35 (6), 1195–1206. https://doi.org/10.1016/0021-9169(73)90016-0.
- Saito, S., Maruyama, T., 2007. Large-scale longitudinal variation in ionospheric height and equatorial spread f occurrences observed by

- ionosondes. Geophys. Res. Lett. 34 (16). https://doi.org/10.1029/2007GL030618
- Schunk, R., Sojka, J.J., 1996. Ionosphere-thermosphere space weather issues. J. Atmos. Terr. Phys. 58 (14), 1527–1574. https://doi.org/ 10.1016/0021-9169(96)00029-3.
- Seba, E.B., Nigussie, M., 2016. Investigating the effect of geomagnetic storm and equatorial electrojet on equatorial ionospheric irregularity over east African sector. Adv. Space Res. 58 (9), 1708–1719. https:// doi.org/10.1016/j.asr.2016.06.037.
- Seba, E.B., Nigussie, M., Moldwin, M.B., 2018. The relationship between equatorial ionization anomaly and nighttime equatorial spread f in East Africa. Adv. Space Res. 62 (7), 1737–1752. https://doi.org/10.1016/j.asr.2018.06.029.
- Sekar, R., Raghavarao, R., 1987. Role of vertical winds on the rayleightaylor mode instabilities of the night-time equatorial ionosphere. J. Atmos. Terr. Phys. 49 (10), 981–985. https://doi.org/10.1016/0021-9169(87)90104-8.
- Stolle, C., Lühr, H., Rother, M., Balasis, G., 2006. Magnetic signatures of equatorial spread f as observed by the champ satellite. J. Geophys. Res.: Space Phys. 111 (A2). https://doi.org/10.1029/2005JA011184.
- Su, S.-Y., Liu, C., Ho, H., Chao, C., 2006. Distribution characteristics of topside ionospheric density irregularities: Equatorial versus midlatitude regions. J. Geophys. Res.: Space Phys. 111 (A6). https://doi.org/ 10.1029/2005JA011330.
- Tsunoda, R., Livingston, R., Rino, C., 1981. Evidence of a velocity shear in bulk plasma motion associated with the post-sunset rise of the equatorial f-layer. Geophys. Res. Lett. 8 (7), 807–810. https://doi.org/10.1029/GL008i007p00807.
- Tsunoda, R.T., 1980. Magnetic-field-aligned characteristics of plasma bubbles in the nighttime equatorial ionosphere. J. Atmos. Terr. Phys. 42 (8), 743–752. https://doi.org/10.1016/0021-9169(80)90057-4.
- Woodman, R.F., La Hoz, C., 1976. Radar observations of f region equatorial irregularities. J. Geophys. Res. 81 (31), 5447–5466. https://doi.org/10.1029/JA081i031p05447.